High-throughput CO_2 capture using PIM-1@MOF based thin film composite membranes

Min Liu,[1] Mitchell D. Nothling,[1] Paul A. Webley,[1] Jianyong Jin,[2]* Qiang Fu,[1,3]* Greg G. Qiao[1]*

[1] Department of Chemical Engineering, The University of Melbourne, Parkville, VIC, 3010, Australia.

[2] School of Chemical Sciences, The University of Auckland, Auckland 1142, New Zealand.

[3] The Centre for Technology in Water and Wastewater (CTWW), the School of Civil and Environmental Engineering, University of Technology Sydney (UTS) NSW 2007 Australia.

Abstract: Carbon capture from power plants represents a powerful technique to mitigate increasing greenhouse gas emissions. In this work, we describe a thin film composite (TFC) membrane incorporating a polymer of intrinsic microporosity (PIM-1) and metal organic framework (MOF) nanoparticles for post-combustion CO_2 capture. The novel TFC membrane design consists of three layers: (1) a CO_2 selective layer composed of a PIM-1@MOF mixed matrix; (2) an ultrapermeable PDMS gutter layer doped with MOF nanosheets; and (3) a porous polymeric substrate. Notably, the PDMS@MOF gutter layer incorporating amorphous nanosheets provides a CO_2 permeance of 10,000−11,000 GPU, suggesting less gas transport resistance in comparison with pristine PDMS gutter layers. In addition, by blending nanosized MOF particles (MOF-74-Ni and NH_2-UiO-66) into PIM-1 to afford a selective layer, the resultant TFC membrane

assembly delivered improved CO_2 permeance of 4,660−7,460 GPU and CO_2/N_2 selectivity of 26−33, compared with a pristine PIM-1 counterpart (CO_2 permeance of 4320 GPU and CO_2/N_2 selectivity of 19). Furthermore, PIM-1@MOF based TFC membranes displayed an enhanced resistance to aging effect, maintaining a stable CO_2 permeance of 900−1,200 GPU and CO_2/N_2 selectivity of 26−30 after aging for 8 weeks. As far as we know, the high CO_2 separation performance presented here is unprecedented for PIM-1 based TFC membranes reported in the open literature.

Keywords: High-throughput, CO_2 capture, thin film composite membrane, polymers of intrinsic microporosity, metal-organic frameworks

***Corresponding Authors:**

Jianyong Jin: j.jin@auckland.ac.nz

Qiang Fu: qiang.fu@uts.edu.au

Greg G. Qiao: gregghq@unimelb.edu.au.

1. Introduction

The escalating level of atmospheric carbon dioxide (CO_2) due to the intensive burning of fossil fuels is a key driver of rapid climate change [1]. To address this, more than 190 governments opted into the Paris Agreement in 2017, committing to limit global warming below 2 °C by 2100 by curbing CO_2 emissions [2]. A reduction in CO_2 emissions of 49% by 2030 has been suggested by the Intergovernmental Panel on Climate Change (IPCC) to meet this imperative target [3]. Such an urgent and Herculean task requires immediate aggressive action. A promising route to achieve this goal is to capture and sequester CO_2 from flue gas in power plants [4, 5]. New technology aimed at capturing CO_2 from flue gas must address several practical and economic challenges: (1) the energy consumption of the applied technology should not be higher than 8% of the total produced power for natural gas fired power plants (with coal close to zero), identified in the latest IPCC report [3]; (2) a high-throughput technology is preferable for dealing with the large volume, low pressure (*ca.* 1 bar) characteristics of post-combustion flue gas [6]; and (3) a high CO_2 extraction selectivity is required due to the low CO_2 concentration (15−16%) in flue gas and high CO_2 removal requirement (50−90%) [7]. Amine scrubbing, once considered the most promising technology for CO_2 capture from power plants, cannot meet these new, strict requirements, due to its expensive, energy-intensive separation processes [7-10]. In contrast, membrane-based separation technology delivers many of the desirable attributes for achieving online CO_2 sequestration, including a small footprint, high-energy efficiency and competitive cost.

Within this domain, thin film composite (TFC) membranes have been recognized as a promising candidate for processing large volume of flue gas [4, 5, 11]. In designing TFC membranes, a target CO_2 permeance above 1,000 GPU (gas permeation units, 1 GPU = 3.35 x 10^{-10} mol m^{-2} s^{-1} Pa^{-1}) coupled with a CO_2/N_2 selectivity of over 20 represents the ideal operating window for economic

CO_2 capture from post-combustion flue gas [6]. Polymers of intrinsic microporosity (PIMs) are attractive materials for the fabrication of ultrapermeable TFC membranes. PIMs provide several advantages for CO_2 capture, such as a high fractional free volume, good mechanical and film-forming properties and excellent processability [12, 13]. However, pristine PIM materials usually suffer several limitations, including severe physical aging over time and low CO_2/N_2 selectivity (< 20), limiting their effectiveness in an industrial setting. In addition, the detrimental aging phenomenon is further exacerbated in TFC assemblies, where the faster physical aging resulted in over 90% drop in CO_2 permeance [14, 15].

To offset these issues, we introduce a straightforward approach to simultaneously enhance the aging resistance and CO_2/N_2 selectivity of PIM-1 based TFC membranes by embedding nanosized, multi-functional metal-organic frameworks (MOFs) into the PIM-1 matrix of the selective layer. When assembled, the resultant TFC membranes deliver a CO_2 permeance of 4,660−7,460 GPU and a CO_2/N_2 selectivity of 26−33 under dry conditions, which is a substantial improvement and well beyond the required economic performance for industrial CO_2 capture. Our investigations further reveal that the embedded MOF nanoparticles can increase the PIM layer rigidity by partially "freezing" PIM chains towards molecular rearrangement and lattice contraction *via* strong interactions between the MOF surface and polymer chains. As a result, the TFC membranes are able to maintain over 30% of their original CO_2 permeance and ~100% of CO_2/N_2 selectivity after aging 2 months in air. This finding represents a significant improvement in anti-aging effect compared with the pristine PIM-1 based membrane (~90% loss in gas permeance). The incorporation of MOF into PIM-based TFC membranes holds promise for optimising this technology for translation into industrial settings.

2. Experimental

2.1 Materials

5,5',6,6'-Tetrahydroxy-3,3,3',3'-tetramethylspirobisindane (TTSBI), 2,3,5,6-tetrafluoroterephthalonitrile (TFTPN, 99%), potassium (II) carbonate (K_2CO_3, 99.995%), anhydrous *N*,*N*-dimethylformamide (anhydrous DMF, 99.8%), copper nitrate hemi(pentahydrate) ($Cu(NO_3)_2 \cdot 2.5H_2O$, ≥98%), zirconium(IV) chloride ($ZrCl_4$, ≥99.9%), nickel(II) nitrate hexahydrate ($Ni(NO_3)_2 \cdot 6H_2O$, ≥98%), 2-Aminoterephthalic acid (NH_2-H_2bdc, 99%), 2,5-dihydroxy-1,4-benzendicarboxylic acid (H_4dobdc, 98%), triethylamine (≥99.9%), and 1,3,5-benzenetricarbonyl trichloride (TMC, 98%) were purchased from Sigma-Aldrich without further purification, except TTSBI and TFTPN were recrystallized before polymerization. Aminopropyl terminated polydimethylsiloxane (NH_2-PDMS-NH_2, M_n = 5.0 kDa) was purchased from Gelest Inc. and used as received. Microporous polyacrylonitrile (PAN) substrates were purchased from SolSep BV (MWCO = 10.0 kDa). Acetonitrile (CH_3CN, 99.7%) was purchased from Ajax Finechem and *N*,*N*-dimethylformamide (DMF, 99.9%) was purchased from PROLABO CHEMICALS, respectively. Chloroform ($CHCl_3$), *n*-hexane (C_6H_{14}, 99%) and methanol (MeOH) were purchased from Chem-Supply. Tetrahydrofuran (THF) was distilled from benzophenone and sodium metal under argon.

2.2 Methods

2.2.1 Synthesis of PIM-1

PIM-1 polymer was synthesized according to our previously reported method [16]. Typically, TTSBI (20.5 g, 60.22 mmol) and TFTPN (12.1 g, 60.22 mmol) were dissolved in 400 mL of anhydrous DMF. Then, 67.0 g of anhydrous K_2CO_3 (482 mmol) was added into the above solution quickly with effective stirring. The resultant mixture was further stirred under argon at 70 °C for

72 h. The crude product was dissolved in THF and precipitated from MeOH to give PIM-1 as a yellow solid. GPC: M_n = 70,600 g mol^{-1}; M_w = 266,300 g mol^{-1} in THF solvent.

2.2.2 Synthesis of MOF-74-Ni nanoparticles

MOF-74-Ni nanoparticles were synthesized according to the reported method [17]. Specifically, 100.0 mg of 2,5-dihydroxyterephthalic acid (H_4dobdc) and 465.0 mg of $Ni(NO_3)_2 \cdot 6H_2O$ were dissolved in a mixture containing 40.0 mL of N,N-dimethylformamide (DMF), 2.7 mL of ethanol and 2.7 mL of water in a 250 mL round bottom flask under N_2 atmosphere. Then, 1.0 mL of triethylamine was added rapidly into the above mixture and further stirred for 2 h. The resultant Ni_2(dobdc) nanoparticles were subsequently collected by centrifugation (7,800 r.p.m), re-dispersed in 25.0 mL of DMF, and heated at 120 °C for 6 h. Finally, the MOF-74-Ni nanocrystals were collected by centrifugation (7,800 r.p.m) and washed with DMF three times to remove unreacted ligands. After that, the MOF-74-Ni nanocrystals were washed with chloroform ($CHCl_3$) over two days, changing $CHCl_3$ every 8 h and finally were re-dispersed MOF-74-Ni nanocrystals in fresh $CHCl_3$ for the fabrication of membranes.

2.2.3 Synthesis of nanosized NH_2-UiO-66 nanoparticles

NH_2-UiO-66 nanoparticles were prepared according to the reported procedure [18]. Typically, 535.9 mg of $ZrCl_4$ and 416.6 mg of NH_2-H_2bdc were added to a mixture containing 30 mL of DMF and 2.0 mL of water. The resultant slurry was sonicated for 10 min and transferred into a Teflon-lined autoclave and heated at 120 °C for 24 h. The NH_2-UiO-66 nanocrystals were collected by centrifugation and washed with 40.0 mL of DMF three times to remove the unreacted ligands. Then the NH_2-UiO-66 nanocrystals were washed with chloroform ($CHCl_3$) over two days,

changing $CHCl_3$ every 8 h and finally were re-dispersed NH_2-UiO-66 nanocrystals in fresh $CHCl_3$ for the fabrication of membranes.

2.2.4 Synthesis of amorphous nanosheets

The amorphous MOF (aMOF) nanosheets were synthesized according to our reported method [19]. Specifically, 36.0 mg of H_4dobdc and 30.0 mg of $Cu(NO_3)_2 \cdot 2.5H_2O$ were dissolved in a mixed solvent containing 4.0 mL of DMF and 4.0 mL of CH_3CN. The mixture was heated at 313 K for 24 h. The aMOF nanosheets were collected by centrifugation (7,800 r.p.m) and washed three times with DMF to remove unreacted ligands. After that, the aMOF nanosheets were washed with tetrahydrofuran (THF) over two days, changing THF every 8 h and finally dried at 120 °C under vacuum for 24 h.

2.2.5 Preparation of aMOF/hexane mixture

The aMOF/hexane mixture was obtained by re-dispersing 30.0 mg of the dried aMOF nanosheets into 1.0 L of n-hexane. The mixture was sonicated for 2 h and the upper transparent green solution was collected by centrifugation (4,000 r.p.m for 20 minutes, 800 mL). The green solution was then concentrated to 400.0 mL by rotary evaporation and resulted in a ~0.36 mg/mL of aMOF nanosheets in hexane.

2.2.6 Fabrication of PDMS@aMOF gutter layer

The PDMS@aMOF gutter layers were fabricated by spin-coating technology. Specifically, 400.0 mg of NH_2-PDMS-NH_2 was dissolved in 20.0 mL of aMOF/hexane stock solution (solution i) and 14.0 mg of 1,3,5-benzenetricarbonyl trichloride (TMC) was dispersed into 0.7 mL of *n*-hexane (solution ii). Then, solutions i and ii were mixed for 2 min and 1.0 mL of the resultant

mixture was spin-coated (1,000 rpm, 10 s) onto a pre-wetted PAN substrate (19.63 cm^2). Finally, the PAN/PDMS@aMOF membranes were dried in vacuum for 24 h at room temperature. All the prepared PAN/PDMS@aMOF membranes were tested their CO_2/N_2 separation performance before fabricating the selective layer.

2.2.7 Preparation of pristine PIM-1 based TFC membranes

PIM-1 based TFC membranes were fabricated *via* spin-coating (1000 r.p.m, 15s) PIM-1 solution (in $CHCl_3$) onto the prepared PDMS@aMOF gutter layers. Specifically, 1.0 g of the synthesized PIM-1 was dissolved in 99.0 g $CHCl_3$ to obtain a 1.0 wt% of PIM-1 solution. Then, 2.0 mL of PIM-1 solution was spin-coated onto the PAN/PDMS@aMOF membranes. The resultant TFC membranes were stored in a container (with methanol inside) for 24 h before gas permeation tests.

2.2.8 Preparation of PIM-1@MOF based TFC membranes

The prepared nanosized MOF particles were dispersed into PIM-1 solution (in $CHCl_3$) to provide a series of suspensions with different MOF mass loading: 5, 10, 15, and 20 wt%, respectively. Then, the PIM-1@MOF suspension was spin-coated (700 r.p.m, 15s) onto the PAN/PDMS@aMOF membranes. The resultant mixed matrix TFC membranes were stored in a container (with methanol inside) for 24 h before gas permeation tests.

2.2.9 Gas permeation tests

Single gas permeation of the prepared PIM-1 based TFC membranes were determined by an in-house built constant pressure variable volume method at 1.0 bar (gauge pressure) and 308 K. Specifically, the TFC membranes were fixed in a Teflon holder and their N_2 and CO_2 permeation

flux were sequentially tested. The gas permeance (Q_i, unit of Q_i is GPU, 1 GPU = 3.35×10^{-10} mol m^{-2} s^{-1} Pa^{-1}) was calculated by equation:

$$Q_i = \frac{V_i}{\Delta p \times A}$$

where V_i is the gas flux of penetrant component i determined by a digital flowmeter (ADM2000, Agilent Technologies), Δp is the across membrane pressure difference and A is the effective membrane area. The ideal selectivity (α*) of gas pairs (i and j) is defined as:

$$\alpha_{ij}^{*} = \frac{Q_i}{Q_j}$$

In addition, all the prepared TFC membranes were used to test their CO_2/N_2 separation performance during the physical aging process at 35 °C in air weekly. The aged TFC membranes were refreshed by methanol vapor and used for testing their CO_2/N_2 separation performance.

2.3. Characterization

The molecular weight of PIM was determined by a PL GPC-50 equipped with 5 mm PL gel Mixed C columns and RI detector, using chloroform as eluent and calibrated using low polydispersity polystyrene standards. Powder X-ray diffraction (XRD) experiments were conducted on a Bruker D8 Advance instrument with Cu Kα radiation (40 kV, 40 mA) with a scanning rate of 0.02°. Scanning electron microscopy (SEM) images were obtained from a FEI Teneo Volumescope (accelerating voltage of 10 kV) and all the samples were pre-coated with gold by a Dynavac Mini Sputter Coater prior to imaging. Attenuated total reflectance Fourier-transform infrared spectroscopy (ATR-FTIR) spectra were recorded on a Nexus 470 Fourier-Transform Infrared Spectrometer (Bruker). The size distribution of the synthesized MOF nanoparticles was determined by a Dynamic Light Scattering (DLS) system *(Micromeritics Elzone 5380).* The N_2

adsorption/desorption isotherms of the synthesized MOF particles were tested on a 3Flex machine (Micromeritics).

3. Results and discussion

3.1 Fabrication and Characterization

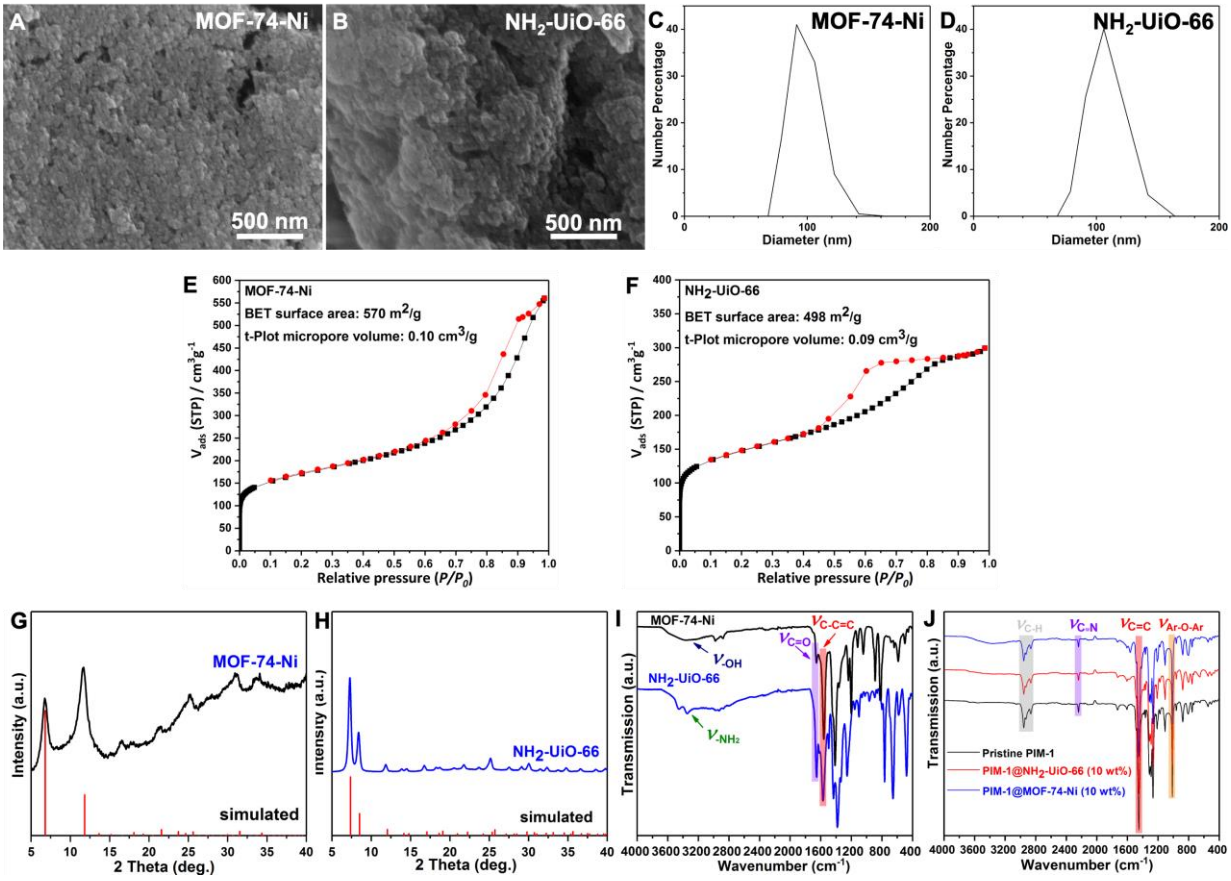

Fig. 1. Scanning electron micrographs (A, B), particle size distributions *via* DLS (C, D), N2 adsorption/desorption isotherms (E, F) powder XRD patterns (G, H), and ATR-FTIR spectra (I) of the synthesized MOF-74-Ni and NH_2-UiO-66 nanoparticles. (J) ATR-FTIR spectra of pristine PIM-1 and PIM-1@MOF based TFC membranes.

Firstly, we aim to prepare nanosized MOF particles as additives to disrupt the chain packing of PIM-1 in the selective layer. MOF-74-Ni and NH_2-UiO-66 MOFs were selected due to their small

in size, high stability toward water,[20] along with the presence of open metal sites (MOF-74-Ni) and -NH_2 functional group. MOF nanoparticles (20−30 nm) were successfully synthesized using an established protocol and confirmed by scanning electron microscopy (SEM) measurements (Fig. 1A and B). The observed MOF nanoparticles display an enlarged hydrodynamic diameter of 100 nm through dynamic light scattering (DLS) measurements, which is attributed to the strong aggregation tendency of nanosized MOF particles in solution (Fig. 1C and D). The Brunauer–Emmett–Teller (BET) surface area of the synthesized MOF-74-Ni and NH_2-UiO-66 particles are 570 m^2/g and 498 m^2/g, respectively. The powder X-ray diffraction (XRD) patterns of the MOF nanoparticles confirmed the crystal structures of MOF-74-Ni and NH_2-UiO-66 (Fig. 1G and H). Specifically, the MOF-74-Ni nanoparticles display two sharp peaks at 6.8° and 11.8°, representing the (120) and (030) crystallographic plane, respectively. The two sharp peaks at 7.3° and 8.5° of the NH_2-UiO-66 nanoparticles correspond to the (111) and (002) crystallographic plane, respectively. The attenuated total reflectance Fourier-transform infrared spectroscopy (ATR-FTIR) spectra show the characteristic C=O (blue region) and C-C=C (red region) stretching vibrations of the prepared MOF particles (Fig. 1I). In addition, the weak, broad peaks between 2800-3600 cm^{-1} represent the stretching vibrations of the amino group (-NH_2) and uncoordinated hydroxy group (-OH) in NH_2-UiO-66 and MOF-74-Ni, respectively. In combination, these results illustrate the successful preparation of crystalline NH_2-UiO-66 and MOF-74-Ni nanoparticles.

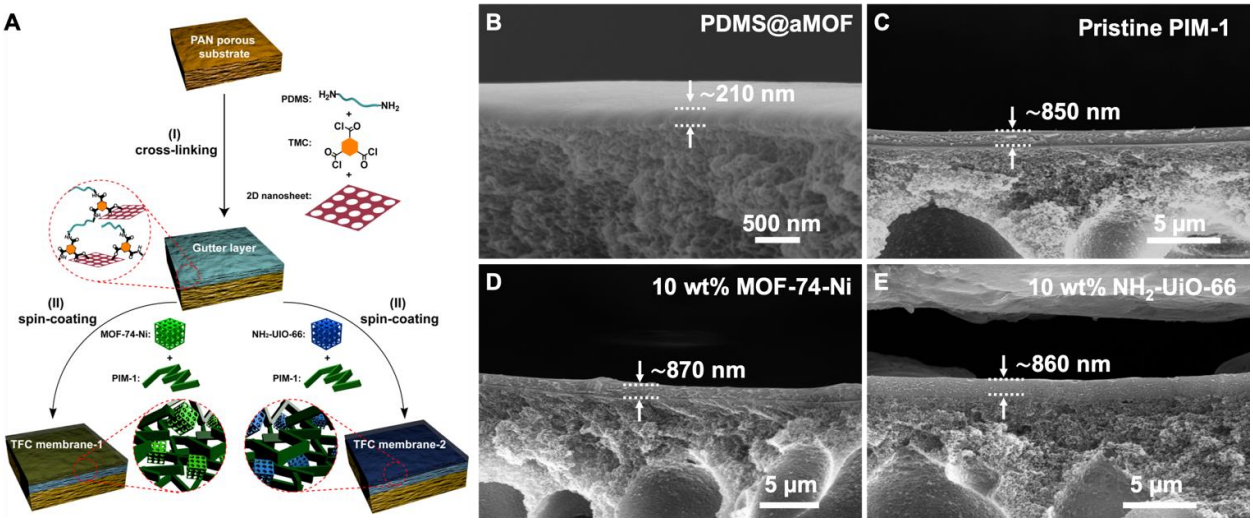

Fig. 2. (A) Fabrication of PIM-1@MOF based TFC membranes: (I) spin-coating a mixture of PDMS and aMOF nanosheets onto a prewetted PAN substrate to afford a gutter layer; (II) spin-coating a PIM-1 and MOF suspension onto the PDMS@aMOF gutter layer to produce a complete TFC membrane. Cross-sectional SEM images of (B) PDMS@aMOF, (C) pristine PIM-1, (D) PIM-1@MOF-74-Ni, and (E) PIM-1@NH_2-UiO-66 based TFC membranes.

We next sought to construct a complete TFC membrane by incorporating the prepared MOF nanoparticles into the PIM-1 selective layer (Fig 2A). Firstly, a thin (~210 nm) gutter layer was prepared by spin-coating a PDMS/aMOF nanosheet composite onto a water prewetted polyacrylonitrile (PAN) substrate (Fig 2B). Next, the complete TFC assembly was fabricated by spin-coating a selective PIM-1 composite layer (with or without MOF nanoparticles) with a

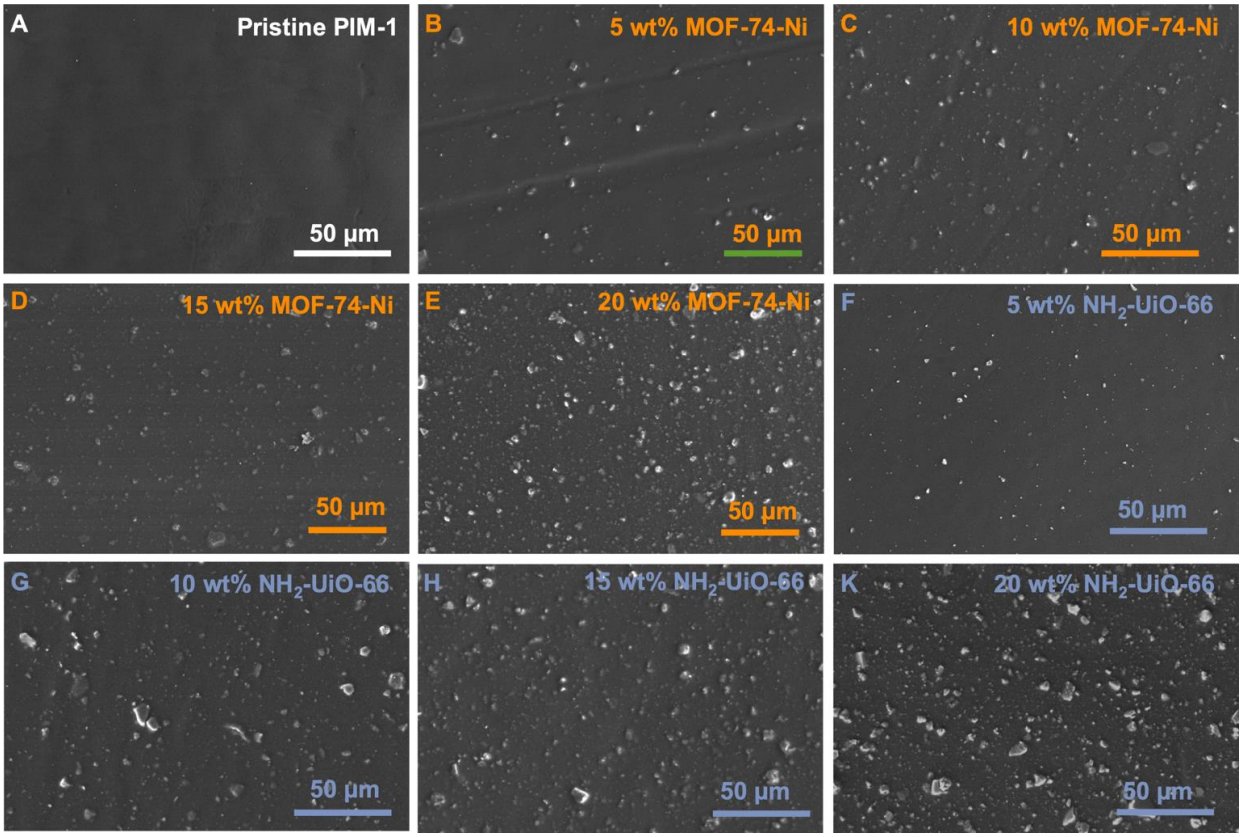

Fig. 3 SEM images of the top surface of prepared PIM-1 based TFC membranes: (A) pristine PIM-1 as a selective layer, (B-E) PIM-1@MOF-74-Ni as a selective layer, and (F-K) PIM-1@NH_2-UiO-66 as a selective layer.

thickness of ~650 nm (determined by subtracting the thickness of the gutter layer), onto the PDMS@aMOF gutter layer (Fig. 2C-E). The pristine PIM-1 based TFC membranes (with 0 wt% MOF loading) display a smooth surface without observable pores or craters (Fig. 3A), which is different from a previous report [21]. This may be attributed to the continuous, strong centrifugal force applied during spin-coating process, resulting in rapid solvent ($CHCl_3$) evaporation and hence preventing the formation of $CHCl_3$ vapor bubbles in the bulk PIM layer. When incorporating MOF nanoparticles at 5 wt%, the resultant TFC membranes exhibit a rough surface, with some MOF nanoparticles observed outside of the PIM matrix. The surface roughness further increased

with higher MOF loadings of 10-20 wt% (Fig. 3B-K). This can be attributed to the aggregation of MOF nanoparticles in the PIM matrix. Examining the fabricated TFC membranes by ATR-FTIR, illustrates the characteristic *Ar*-O-*Ar* (orange region), aromatic C=C (red region), C≡N (violet region), and aliphatic C-H (grey region) stretching vibrations characteristic of PIM-1 polymers (Fig. 1J). However, no significant difference is observed between the PIM-1@MOF composites and pure PIM-1 ATR-FTIR spectra. This may can be attributed to the limited chemical surface contacts of specific MOF nanocrystals with PIM-1 polymers in the bulk PIM phase [17].

3.2 Gas Separation Performance

Following the successful preparation of PIM-1 based TFC membranes, we next evaluated their CO_2/N_2 separation performance. The prepared PAN/PDMS@aMOF gutter layer exhibited outstanding CO_2 permeance of 10,000−11,000 GPU and a CO_2/N_2 selectivity of 9.0−9.5, providing a solid base for the separation performance of the top selective layer. Using pristine PIM-1 as a selective layer, the resultant fresh TFC membranes exhibited a CO_2 permeance of 4,320 GPU and CO_2/N_2 selectivity of 19. However, we observed a significant loss in CO_2 permeance (from 4,320 GPU to 1,400 GPU, *ca.* 68%) along with an enhancement in CO_2/N_2 selectivity (from 19 to 35) after one week (Fig. 4C and D), which is known to be due to a rapid physical aging effect. The CO_2 permeance dropped further to ~490 GPU, plateauing at *ca.* 10% of the fresh membrane permeance after aging for three weeks. Indeed, physical aging commonly occurs in glassy polymers due to the nonequilibrium state of polymer chains after the removal of solvents. This phenomenon is manifested by a continuous, spontaneous molecular rearrangement and lattice contraction within the polymer matrix towards equilibrium at temperatures well below their glass transition temperatures. This results in a reduction of free volume and gas permeability, with an accompanying increase in gas-pair selectivity [22, 23].

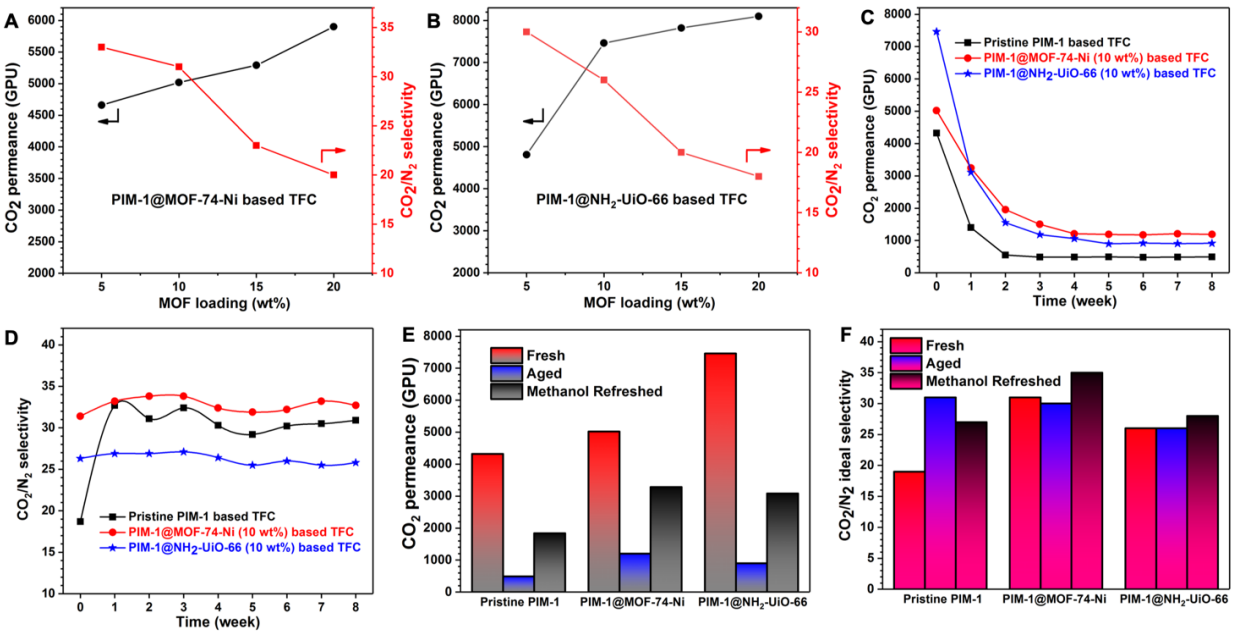

Fig. 4 CO_2/N_2 separation performance of fresh (A) PIM-1@MOF-74-Ni and (B) PIM-1@NH_2-UiO-66 based TFC membranes. The CO_2/N_2 separation performance of pristine PIM-1, PIM-1@MOF-74-Ni (10 wt%), and PIM-1@NH_2-UiO-66 (10 wt%) based TFC membranes during aging at 35 °C in air over 8 weeks: (C) CO_2 permeance and (D) CO_2/N_2 selectivity. The comparison of CO_2/N_2 separation performance between fresh and methanol refreshed PIM-1 based TFC membranes: (E) CO_2 permeance and (F) CO_2/N_2 selectivity.

When loading the PIM-1 selective layer with 5 wt% MOF-74-Ni, an approximate 8% enhancement in CO_2 permeance (4,660 GPU *vs.* 4,320 GPU) and a >70% increase in CO_2/N_2 selectivity (from 19 to 33) was observed compared with a TFC membrane with a pristine PIM-1 selective layer (Fig. 4A). The simultaneous increase in both CO_2 permeance and CO_2/N_2 selectivity is therefore attributed to the incorporation of MOF nanoparticles into PIM-1 matrix, leading to an increase in free volume and hence improve gas permeation rates. In addition, the uncoordinated metal (Ni^{2+}) sites and -OH groups of the MOF-74-Ni nanoparticles can have strong interactions with PIM-1 chains, forming a higher concentration of CO_2 selective regions at the layer interface.

Further enhancement in CO_2 permeance (>5,000 GPU) was observed when increasing the MOF-74-Ni loading to 10 wt%, with a similar improved CO_2/N_2 selectivity of 31. However, further increases in MOF-74-Ni loading leads to a drop in CO_2/N_2 selectivity due to the aggregation of MOF nanoparticles, resulting in non-selective regions in the selective layer matrix (Fig. 4A). Of particular note, the PIM-1@MOF-74-Ni (10 wt%) TFC membrane exhibited a reduced loss in CO_2 permeance (from 5,020 GPU to 3,240 GPU, *ca.* 35%) after aging one week in air at 35 °C. This enhanced resistance to aging can be attributed to the introduction of nanosized, multi-functional MOF nanoparticles into PIM-1, leading to strong interactions (*e.g.* hydrogen bonding) between the polymer chains and MOF surfaces.[18, 24] Through these interactions, PIM-1 chains are rigidified, mitigating the trend toward molecular rearrangement and lattice contractions within the PIM matrix. As a result, CO_2 permeance of the PIM-1@MOF-74-Ni membrane could be maintained at ~1,200 GPU with negligible change in CO_2/N_2 selectivity (30) after 8 weeks of aging (Fig. 4C and D). This separation performance is well positioned in the economic target area for post-combustion CO_2 capture suggested by Merkel *et al.* (Fig. 5) [6].

To assess the effect of MOF structure on PIM-1@MOF membrane performance, TFC membranes were prepared with varied loadings of the alternative MOF nanoparticle, NH_2-UiO-66. Nanosized NH_2-UiO-66 MOF particles have been explored previously to enhance gas permeation selectivity and aging resistance in mixed matrix membranes (MMMs) [18]. However, the resistance to aging of a TFC assembly normally departs significantly from that observed under a dense MMM regime [22, 25]. Therefore, a PIM-1@NH_2-UiO-66 composite was coated onto PAN/PDMS@aMOF substrates to investigate its anti-aging performance in a TFC membrane system. With 5 wt% loading of NH_2-UiO-66 MOF particles into the PIM-1 selective layer, similar CO_2 permeance (4,810 GPU *vs.* 4,660 GPU) and CO_2/N_2 selectivity (30 *vs.* 33) was observed to

that of the equivalent PIM-1@MOF-74-Ni based TFC membranes. Furthermore, CO_2 permeance increased to 7,460 GPU with a higher MOF loading of 10 wt%, while maintaining CO_2/N_2 selectivity ratio of 26. However, the PIM-1@NH_2-UiO-66 (10 wt%) TFC membrane exhibited a significant reduction in CO_2 permeance after aging for one week compared to that observed for the MOF-74-Ni (10 wt%) TFC system (58% *vs.* 35%). The CO_2 permeance and CO_2/N_2 selectivity plateaued at ~900 GPU and ~26, respectively after aging for four weeks. Increases to the MOF mass loading (15-20 wt%) resulted again in particle aggregation, the presence of more defects in the PIM-1 layer and reduced separation performance (Fig. 4D). Of particular note, after physical aging, the PIM-1@MOF-74-Nibased TFC membrane showed higher CO_2 permeance than that of PIM-1@NH_2-UiO-66 counterpart (1200 GPU *vs.* 900 GPU). This may be due to the difference in MOF structure properties, *i.e.* the open metal sites within MOF-74-Ni may have stronger interactions than the hydrogen bonding of -NH_2 within NH_2-UiO-66, leading to less structural collapse of PIM-1 matrix.

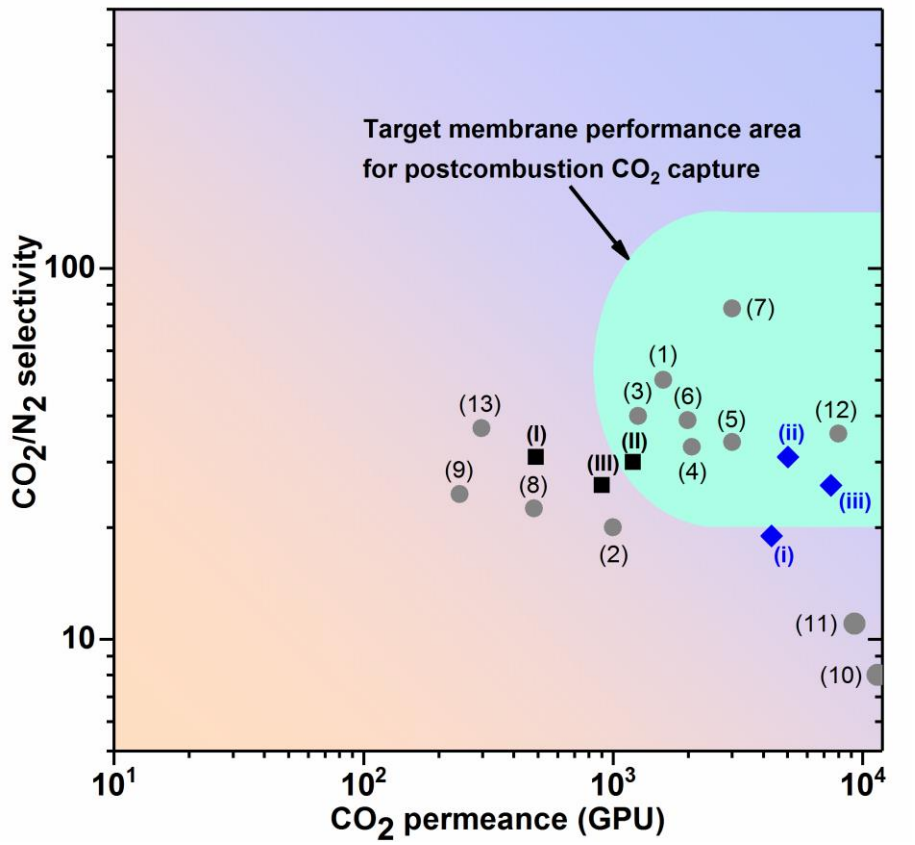

Fig. 5 Comparison of CO_2/N_2 separation performance by state-of-the-art TFC membranes. Facilitated transport membranes are excluded and the target area for post-combustion CO_2 capture (turquoise) is referred from Merkel *et al*. [6]. Specific details have been summarized in Table 1.

Table 1. Comparison of the CO_2/N_2 separation performance of the state-of-art thin film composite membranes.

Reference	Membrane configuration			CO_2 permeance [GPU]/CO_2/N_2 ideal selectivity	
	Selective layer	Gutter layer	Support	**Fresh**	**Aged***
(1) Energy Environ. Sci. 2011, 4, 4656	Polyactive®	PDMS	PAN	1590/50	N/A
(2) J. Mater. Chem. A 2015, 3, 14876	Pebax®2533/SNP1	PDMS	PAN	1000/20	N/A
(3) Energy Environ. Sci. 2016, 9, 434	PEG	PDMS	PAN	1260/40	N/A
(4) ACS Nano 2018, 12, 11591	Polyactive®	2D MOF	PAN	2070/33	N/A
(5) Energy Environ. Sci. 2018, 11, 544	PEG	3D MOF	α-Al_2O_3	3000/34	N/A
(6) J. Mater. Chem. A 2019,	PEG	PDMS@aMOF	PAN	1990/39	N/A
(7) Nat. Mater. 2019, 18, 163	MMP	PDMS	PSF	3000/78	N/A
(8) J. Membr. Sci. 2018, 563, 93	PIM-CD	PDMS	PAN	483/22.5	N/A
(9) J. Membr. Sci. 2013, 156, 169	PIM-1/Matrimid	N/A	PSF	243/24.6	N/A
(10, 11) J. Membr. Sci. 2018, 564, 878	PIM-1/C-HCP	N/A	PAN	~11500/~8	>9300/11
(12, 13) J. Mater. Chem. A 2019, 7, 6417	PIM-1	PTMSP	MFFK-1	8010/35.8	297/37.1
(i, I) This work	PIM-1	PDMS@aMOF	PAN	4320/19	490/31
(ii, II) This work	PIM-1/MOF-74-Ni	PDMS@aMOF	PAN	5018/31	1200/30
(iii, III) This work	PIM-1/NH_2-UiO-66	PDMS@aMOF	PAN	7460/26	900/26

* Entries (1-6) are rubbery poly(ethylene glycol) (PEG) or poly(ethylene oxide) (PEO) based TFC membranes, which rarely show aging phenomenon. Entry (7) is ordered microporous polymer based TFC membrane without aging limitation. The aging data of entries (8) and (9) are not available from the literature.

A comparison of CO_2/N_2 separation performance of the PIM-1@MOF membranes against state-of-the-art TFC membranes is shown in Fig. 5 and detailed in Table 1. The freshly prepared PIM-1@MOF TFC membranes exhibit outstanding gas permeance than previously reported TFC assemblies, in combination with competitive CO_2/N_2 selectivity values. An exception is the recent work of Borisov *et al* [14], poly[1-trimethylsilyl-1-propyne] (PTMSP) with extremely high CO_2 permeability ($\geq$19,000 Barrer) was employed as a gutter layer [26, 27], However, the aged PTMSP-based membranes suffer from a significant drop in CO_2 permeance to 208−297 GPU, suggesting a more severe aging effect contributed by the PTMSP gutter layer [14], In the current study, we employ an ultrapermeable and stable PDMS@aMOF gutter layer, which has several benefits in TFC membrane construction. In particular, the flexible, rubbery nature of the PDMS@aMOF ensures that it offers minimal contribution to the overall membrane gas transport resistance during the aging process gutter [28, 29]. Indeed, the primary contributor to the reduced permeance with aging in the current systems comes from the composite PIM@MOF selective layers. However, this effect can be partially offset by exposing the physically aged PIM-1@MOF TFC membranes to methanol vapor. Interestingly, the methanol-refreshed TFC membranes recover over 40% of their original CO_2 gas permeance (3,290 or 3,080 GPU for MOF-74-Ni or NH_2-UiO-66 based TFC membranes, respectively) with only a slight increase in CO_2/N_2 selectivity (Fig. 4E and F). This is due to the methanol vapor can diffuse into PIM-1 polymer matrix and expand the collapsed the chain structures.

4. Conclusions

In conclusion, we have prepared a series of PIM-1@MOF TFC membranes with high CO_2/N_2 separation performance *via* a straightforward spin-coating approach. In the presented TFC design, we employed a composite PDMS@aMOF gutter layer, which provides significantly reduced gas transport resistance in contrast to pristine PDMS gutter layers. Outstanding CO_2 permeance of the gutter layer (10,000−11,000 GPU), combined with a CO_2/N_2 selectivity of 9.0−9.5 contributes to the high performance of the complete TFC membranes. Thereafter, nanosized MOF particles (MOF-74-Ni and NH_2-UiO-66) were incorporated into a PIM-1 matrix and the resultant TFC membranes exhibited enhanced CO_2 permeance (4,660−7460 GPU) as well as CO_2/N_2 selectivity (26−33) compared to pristine PIM-1-based TFC membranes. In addition, while pristine PIM-1 suffers from a rapid loss in gas permeance with aging, the PIM-1@MOF membranes provide significantly improved resistance to aging, maintaining high CO_2 permeance (900−1,200 GPU) and CO_2/N_2 selectivity (26−30) after aging for two months. To the best of our knowledge, this separation performance exceeds that of any previously reported PIM-1 based TFC membranes, highlighting the promise of this approach for economic post-combustion CO_2 capture. This study therefore opens a new avenue for the optimisation of glassy polymer based TFC membranes for industrial application.

Conflicts of interest

The authors declare no competing financial interest.

Acknowledgements

The authors appreciate the Bio21 Advanced Microscopy Facility for the assistance with material characterization and Mr. Gan Lin for the DLS tests. Min Liu acknowledges the support from China Scholarship Council – The University of Melbourne Scholarship (201606260063), Particulate

Fluids Processing Centre (PFPC), and Salis Institute (Steps to Independence Grant). articulate Fluids Processing Centre (PFPC). Qiang Fu acknowledges the Australian Research Council under the Future Fellowship (FT180100312).

References

[1] J. Tollefson, Clock ticking on climate action, Nature 562 (2018) 172.
[2] United nations framework convention on climate change, adoption of the paris agreement, UNFCCC Secretariat Bonn2015.
[3] Summary for policymakers of ipcc special report on global warming of 1.5 °c approved by governments, Intergovernmental Panel on Climate Change2018.
[4] R.W. Baker, B.T. Low, Gas separation membrane materials: A perspective, Macromolecules 47 (2014) 6999-7013.
[5] M. Liu, M.D. Nothling, P.A. Webley, Q. Fu, G.G. Qiao, Postcombustion carbon capture using thin-film composite membranes, Acc. Chem. Res. 52 (2019) 1905-1914.
[6] T.C. Merkel, H. Lin, X. Wei, R. Baker, Power plant post-combustion carbon dioxide capture: An opportunity for membranes, J. Membr. Sci. 359 (2010) 126-139.
[7] D.M. D, Carbon dioxide capture: Prospects for new materials, Angew. Chem. Int. Ed. 49 (2010) 6058-6082.
[8] G.T. Rochelle, Amine scrubbing for co2 capture, Science 325 (2009) 1652-1654.
[9] D. Cebrucean, V. Cebrucean, I. Ionel, Co2 capture and storage from fossil fuel power plants, Energy Procedia 63 (2014) 18-26.
[10] E.S. Rubin, J.E. Davison, H.J. Herzog, The cost of co2 capture and storage, International Journal of Greenhouse Gas Control 40 (2015) 378-400.
[11] H.B. Park, J. Kamcev, L.M. Robeson, M. Elimelech, B.D. Freeman, Maximizing the right stuff: The trade-off between membrane permeability and selectivity, Science 356 (2017) 1137.
[12] R.S. Bhavsar, T. Mitra, D.J. Adams, A.I. Cooper, P.M. Budd, Ultrahigh-permeance pim-1 based thin film nanocomposite membranes on pan supports for co2 separation, J. Membr. Sci. 564 (2018) 878-886.
[13] P.M. Budd, E.S. Elabas, B.S. Ghanem, S. Makhseed, N.B. McKeown, K.J. Msayib, C.E. Tattershall, D. Wang, Solution‐processed, organophilic membrane derived from a polymer of intrinsic microporosity, Adv. Mater. 16 (2004) 456-459.
[14] I. Borisov, D. Bakhtin, J.M. Luque-Alled, A. Rybakova, V. Makarova, A.B. Foster, W.J. Harrison, V. Volkov, V. Polevaya, P. Gorgojo, Synergistic enhancement of gas selectivity in thin film composite membranes of pim-1, J. Mater. Chem. A 7 (2019) 6417-6430.
[15] A.K. Sekizkardes, V.A. Kusuma, J.S. McNally, D.W. Gidley, K. Resnik, S.R. Venna, D. Hopkinson, Microporous polymeric composite membranes with advanced film properties: Pore intercalation yields excellent co 2 separation performance, J. Mater. Chem. A 6 (2018) 22472-22477.
[16] P. Yanaranop, B. Santoso, R. Etzion, J. Jin, Facile conversion of nitrile to amide on polymers of intrinsic microporosity (pim-1), Polymer 98 (2016) 244-251.
[17] J.E. Bachman, J.R. Long, Plasticization-resistant ni2(dobdc)/polyimide composite membranes for the removal of co2 from natural gas, Energy Environ. Sci. 9 (2016) 2031-2036.

[18] B. Ghalei, K. Sakurai, Y. Kinoshita, K. Wakimoto, Ali P. Isfahani, Q. Song, K. Doitomi, S. Furukawa, H. Hirao, H. Kusuda, S. Kitagawa, E. Sivaniah, Enhanced selectivity in mixed matrix membranes for co2 capture through efficient dispersion of amine-functionalized mof nanoparticles, Nat. Energy 2 (2017) 17086.
[19] L. Min, X. Ke, M.D. Nothling, Z. Lianhai, f. qiang, P.A. Webley, G.G. Qiao, Ultrapermeable thin film composite membranes enhanced via doping mof nanosheets, 2020.
[20] M.J. Kalmutzki, C.S. Diercks, O.M. Yaghi, Metal–organic frameworks for water harvesting from air, Adv. Mater. 30 (2018) 1704304.
[21] C.Z. Liang, J.T. Liu, J.-Y. Lai, T.-S. Chung, High-performance multiple-layer pim composite hollow fiber membranes for gas separation, J. Membr. Sci. 563 (2018) 93-106.
[22] Y. Huang, D.R. Paul, Physical aging of thin glassy polymer films monitored by gas permeability, Polymer 45 (2004) 8377-8393.
[23] Y. Huang, D.R. Paul, Experimental methods for tracking physical aging of thin glassy polymer films by gas permeation, J. Membr. Sci. 244 (2004) 167-178.
[24] J.E. Bachman, Z.P. Smith, T. Li, T. Xu, J.R. Long, Enhanced ethylene separation and plasticization resistance in polymer membranes incorporating metal–organic framework nanocrystals, Nat. Mater. 15 (2016) 845-849.
[25] R.R. Tiwari, J. Jin, B. Freeman, D. Paul, Physical aging, co2 sorption and plasticization in thin films of polymer with intrinsic microporosity (pim-1), J. Membr. Sci. 537 (2017) 362-371.
[26] T. Masuda, Y. Iguchi, B.-Z. Tang, T. Higashimura, Diffusion and solution of gases in substituted polyacetylene membranes, Polymer 29 (1988) 2041-2049.
[27] L. Robeson, W. Burgoyne, M. Langsam, A. Savoca, C. Tien, High performance polymers for membrane separation, Polymer 35 (1994) 4970-4978.
[28] K. Xie, Q. Fu, C. Xu, H. Lu, Q. Zhao, R. Curtain, D. Gu, P.A. Webley, G.G. Qiao, Continuous assembly of a polymer on a metal–organic framework (cap on mof): A 30 nm thick polymeric gas separation membrane, Energy Environ. Sci. 11 (2018) 544-550.
[29] M. Liu, K. Xie, M.D. Nothling, P.A. Gurr, S.S.L. Tan, Q. Fu, P.A. Webley, G.G. Qiao, Ultrathin metal-organic framework nanosheets as a gutter layer for flexible composite gas separation membranes, ACS Nano 12 (2018) 11591-11599.

For TOC only

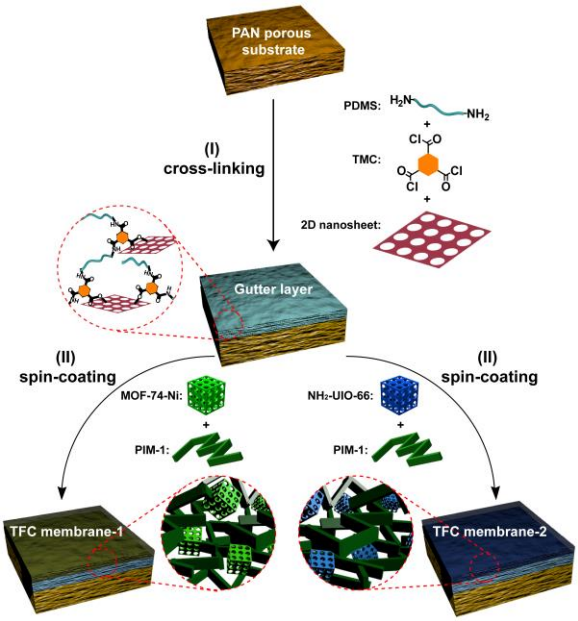
PAN porous substrate
PDMS:
TMC:
2D nanosheet:
(I) cross-linking
Gutter layer
(II) spin-coating
MOF-74-Ni:
PIM-1:
(II) spin-coating
NH2-UIO-66:
PIM-1:
TFC membrane-1
TFC membrane-2